J. Wind Eng. Ind. Aerodyn. 98 (2010) 377–385

Contents lists available at ScienceDirect

Journal of Wind Engineering and Industrial Aerodynamics

journal homepage: www.elsevier.com/locate/jweia

Lateral channeling within rectangular arrays of cubical obstacles

Marko Princevac [a,*], Jong-Jin Baik [b], Xiangyi Li [a], Hansheng Pan [a], Seung-Bu Park [b]

[a] Department of Mechanical Engineering, University of California at Riverside, Bourns Hall A368, Riverside, CA 92521, USA
[b] School of Earth and Environmental Sciences, Seoul National University, Seoul 151-747, Republic of Korea

ARTICLE INFO

Article history:
Received 25 August 2007
Received in revised form
31 October 2009
Accepted 5 November 2009
Available online 9 December 2009

Keywords:
Urban flow
Building array: Lateral channeling
Water channel
Physical modeling
Particle image velocimetry
PIV

ABSTRACT

Water channel experiments were conducted with the goal of obtaining better understanding of flows through urban-like arrays of buildings. Particle Image Velocimetry (PIV) was used for comprehensive flow measurements within a modeled simple urban setup. Building arrays were modeled using acrylic blocks whose refractive index is the same as that of salty water. Such a setup allowed for undisturbed laser sheet illumination through the obstacles enabling detailed flow measurements between the obstacles/buildings. Building array size, measurement plane and flow conditions were varied. A novel flow feature, lateral channeling, observed and quantitatively measured, within regular 3×3 and 5×5 arrays of cubes is reported here. A sideways mean outflow from the building array is observed behind the first row of buildings followed by the mean inflow in the lee of all succeeding rows of buildings. When the central building in a 3×3 array is replaced by a building of double height, due to the strong downdraft caused by this tall building, the lateral outflow becomes significantly more intense. When the central building in a 5×5 array is replaced by a building of double height, the building downdraft blocks the lateral inflow to the array. This is the first time that such detailed measurements are available for a mock urban array of finite size—a real three-dimensional case. The newly identified mean flow pattern may be accountable for the initial plume spread within an array of obstacles.

1. Introduction

Urban areas of the world are experiencing rapid growth which raises concerns of environmental deterioration, degradation of life quality and possibility of a deliberate toxic release. One of the central urban problems is the dynamics of environmental flows, their nature and transport and mixing capabilities (Fernando et al., 2001). Although significant progress has been made on understanding urban flow phenomena, a variety of issues remain to be understood. Most of the past studies on urban flow and dispersion can be classified in several groups: studies on flow above roughness elements, studies related to flows around individual buildings, street canyon flow studies and studies on urban canopy flow as a whole. There are numerous field, laboratory and numerical agriculture-related studies dealing with flows above and inside the vegetative canopy (e.g. Shavit and Brandon, 2001; Takahashi and Hiyama, 2004; Finnigan and Belcher, 2004) which may have similarities with flows inside and above the urban canopy. Some relevant urban oriented studies are given next.

Detailed laboratory experiments with a focus on the flow readjustment to a different surface roughness were conducted by Cheng and Castro (2002a). Using wind-tunnel experiments, Cheng and Castro (2002b) investigated the spatially averaged mean velocity and turbulent stresses above an urban-like surface. This study pointed out some difficulties in applying the fore mentioned results of flows over vegetative canopies to flows above urban canopies.

Hosker (1980) provided a review of studies related to isolated buildings. Extensive investigations of flows around single building and flows in complex scaled city blocks were conducted in a wind tunnel (e.g. Pavageau and Schatzmann, 1999; Schatzmann et al., 2000). Those studies examined the turbulent characteristics of the flows and the statistical properties of concentration fields associated with steady releases at street level. Similar studies were conducted to examine flow and dispersion around scaled model buildings using EPA's fluid modeling facility (Brown et al., 2001).

Some studies of flow and dispersion within the urban canopy have modeled the canopy as a series of urban street canyons. Oke (1987) summarized the nature of this flow in terms of the ratio of the spacing between buildings, S, to the building height, H. Based on past studies conducted in wind tunnels and water flumes, Oke defines three types of flow regimes depending on S/H: isolated roughness flow regime for $S/H > 4$, wake

* Corresponding author. Tel.: +1 951 827 2445; fax: +1 951 827 2899.
E-mail address: marko@engr.ucr.edu (M. Princevac).

0167-6105/$ - see front matter © 2009 Elsevier Ltd. All rights reserved.
doi:10.1016/j.jweia.2009.11.001

interference flow regime for $2 < S/H < 4$, and the skimming flow regime for $S/H < 2$.

Other studies have focused on individual street canyons and street intersections, where complex flow patterns can occur. Kastner-Klein et al. (2001) used a wind tunnel, while Macdonald et al. (2002) used a water flume to study the details of such flows. Yamartino and Wiegand (1986), Gavze et al. (2002), and Rotach et al. (2005) conducted field studies in which turbulence intensities and flow velocities were measured with sonic anemometers, and the associated concentration patterns were studied using tracer releases. Such studies have provided useful insight into urban street canyon flows. In a narrow street canyon ($S/H \sim 1$), a single horizontally aligned in-canyon vortex develops, while a smaller counter-rotating vortex may develop next to it in a wider canyon ($S/H \sim 1.5$). Baik et al. (2000) and Eliasson et al. (2006) tried to elucidate the vertical structure of the flow inside deep canyons ($S/H < 0.5$). Different studies have looked at the effect of roof shape and relative building heights on vertical transport and dispersion (e.g. Rafailidis and Schatzmann, 1995; Kastner-Klein et al., 1997; Macdonald et al., 1998). A number of wind tunnel tracer experiments have shown that concentrations for releases in the street canyon are particularly sensitive to the approaching wind direction (Wedding et al., 1977; Hoydysh and Dabberdt, 1988; Kastner-Klein and Plate, 1999). Dabberdt and Hoydysh (1991) found that concentrations within the street canyon vary significantly with block shape (rectangular vs. square) and with the relative width of streets vs. avenues.

The influence of street architecture on the wind and turbulence patterns in street canyons and the associated effects on local air quality were also studied (Kastner-Klein et al., 2004; Kastner-Klein and Rotach, 2004, etc.). The results suggest that small-scale features of the building architecture (e.g. roof) may play an important role in determining canyon flow patterns.

Reduced-scale field experiments and water flumes were used to study the interaction of a tracer plume with the internal boundary layer created over the obstacle array (Macdonald et al., 2000a, b; Macdonald, 2000). Compared to plumes in the open terrain, the plumes in the arrays were typically wider, and the plume width was closely related to the width of the obstacles. It was found that the lateral concentration profiles were Gaussian in all cases when the wind was perpendicular to the obstacle array. However, plumes were deflected along street canyons when the wind direction was not normal to the array.

Yee et al. (2006) compared results from field tracer measurements with corresponding simulations using a water channel and a wind tunnel. They found that the field measurements agree better with the water channel measurements than with the wind tunnel results. The better performance of the water channel might be related to the more precise flow control and conditioning that is possible in the water channel.

Coceal et al. (2006) performed the direct numerical simulations (DNS), while Lien and Yee (2004) deployed the $k-\varepsilon$ model to study flows through regular arrays. Lien et al. (2005) presented the mathematical foundation for modeling the flow within three-dimensional building arrays. Theurer et al. (1996) made the wind tunnel investigation of several hierarchical, idealized, arrangements of buildings to obtain the parameters required in a semi-empirical urban dispersion model. The wind tunnel experiments showed that the influence of individual obstacles becomes negligible at downwind distances larger than the radius of homogenization (ROH). At distances larger than ROH, for the dispersion calculation, buildings can be considered as homogeneous roughness. It should be mentioned that one of the motivations for the present laboratory study was validation and improvements of another semi-empirical model, the Quick Urban and Industrial Complex (QUIC) model. Theurer (1999) proposed a classification scheme for urban environments which consists of nine typical building arrangements. The effect of each building arrangement on local concentration of pollutants was investigated through wind tunnel experiments and numerical modeling. However, due to the complex interactions of the flow and buildings no explicit formula for the concentration in terms of different building parameters was possible.

Several major field measurements related to the urban flows and dispersion were conducted. These field campaigns include the Urban 2000 (Salt Lake City, Utah, Allwine et al. 2002), Mock Urban Setting Test-MUST (Biltoft, 2001), Joint Urban 2003 (JU2003, Oklahoma City, Oklahoma, Allwine et al., 2004), and the New York City Urban Dispersion Program (Allwine and Flaherty, 2006). Similar field measurements were conducted in European cities, e.g. the Basel Urban Boundary Layer Experiment (BUBBLE, Rotach et al., 2005). These campaigns resulted in invaluable data sets but measurements are site specific and due to the complexity of urban morphology it is not trivial to generalize them.

Over the past several years, a group at the University of California at Riverside (UCR) has conducted several tracer studies to understand flow and dispersion in urban areas. In one of them, a model urban area was constructed on the Dugway Proving Ground using meter high drums (Yuan and Venkatram, 2005). Tracer sampling on several arcs within the model canopy was supplemented with turbulence measurements. The study showed that tracer concentrations could be estimated well if flow and turbulence within the canopy were measured. In another study (Venkatram et al., 2005) a tracer was released from the top of a trailer surrounded by buildings. The major finding from this study was that surrounding buildings induce large horizontal fluctuations leading to dispersion that could not be estimated using conventional dispersion models. All studies pointed to the need to understand the details of the interaction of the mean flow with urban morphology.

What is lacking is a systematic study of flow in building clusters of varying complexity. To address this gap we initiated a systematic experimental program in the newly established Laboratory for Environmental Flow Modeling (LEFM) at UCR. As a part of the study, in this communication we present a new mean flow pattern through regular arrays of cubical obstacles in the skimming regime. The laboratory setup and its capabilities are described in Section 2 followed by the experimental results in Section 3. Results are summarized in Section 4.

2. Laboratory setup

A custom-designed circulating water channel, with a test section that is 1.5 m long, 1 m wide and 0.5 m deep (Fig. 1), was utilized for the experiments. Water is circulated through the test section using a 20 HP axial pump, which produces a maximum mean velocity of $0.5\,\mathrm{m\,s^{-1}}$ in the test section. A variable frequency controller allows flow control with a resolution of 1/100 Hz (from 0 to 60 Hz) which corresponds to the mean velocity change resolution of only $0.08\,\mathrm{mm\,s^{-1}}$. Flow conditioning is achieved with the profiled honeycombs and the custom-built perforated screens. The perforated screens are used to generate desired inflow velocity profiles as a part of the flow conditioning. The channel flow is steady and becomes fully developed before reaching the test section.

The LEFM is equipped with the Particle Image Velocimetry (PIV) system for velocity measurements. Detailed velocity field can be measured in the vertical or horizontal plane. PIV measurement technique is well established and widely used for fluid flow investigations (Adrian, 1988, 1991, 1997; Prasad et al., 1992).

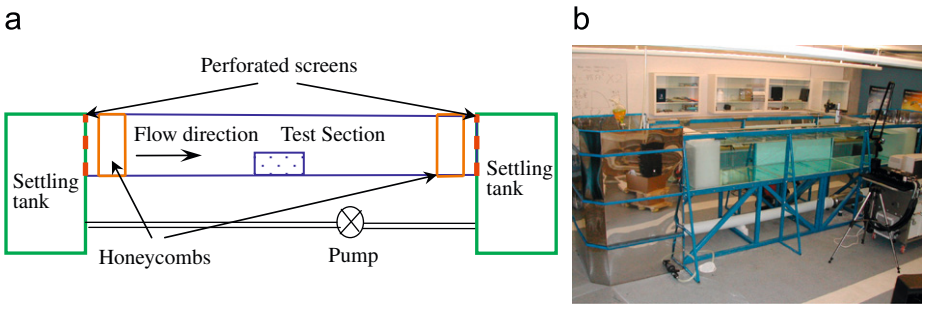

Fig. 1. (a) Schematic (side view) and (b) photograph of the water channel.

The channel has flow control capability to maintain desired velocity profile starting from the classical logarithmic to the linear profile. As needed, the channel can also maintain well-defined jets at desired height. Experiments presented in this paper are all with the logarithmic mean velocity profile. Vertical profiles of the standard deviations of vertical and horizontal velocities, σ_u and σ_w, were maintained constant (around 0.028 and 0.018 m s^{-1}, respectively) with σ_u exhibiting a slight peak (0.032 m s^{-1}) at 1 cm from the ground. The flow becomes Reynolds number independent for the pump setting larger than 30 Hz (50% of the pump capacity), which corresponds to the Reynolds number, based on the obstacle height, Re=5000.

The model buildings are made of highly polished acrylic. Flow is seeded with the Pliolite® particles with the median diameter of 50 μm. The particles are rendered neutrally buoyant by adding filtered and re-crystallized salt of high purity (Morton Culinox 999) to the water. In addition to increasing the density, the salt brings the refractive index of the water closer to that (Aly and Esmail, 1993) of the acrylic used to construct the model buildings. This minimizes the refraction of the laser sheet which, depending on the experimental configuration, has to pass through several building rows. This study is the first that reports results of detailed PIV measurements through and within arrays of obstacles and cover the whole horizontal field at once with no blind spots.

3. Laboratory measurements

Simple experimental series with a single cubical obstacle were used to validate the newly built water channel setup since these are well-known canonical flows. These measurements did not bring any new results but served to confirm the validity of the PIV measurements by comparing them with already known flow patterns. An investigation of the vertical flow field through and above a 3 × 3 cubical array also did not convey anything new. However, when we initiated the measurements of the horizontal flow field through a regular 3 × 3 array of cubes an interesting mean flow pattern was observed.

In this communication we focus on the mean flow feature which was first noticed while investigating a regular 3 × 3 array of cubical obstacles in the skimming regime. Results of the mean flow measurements through a regular 5 × 5 array are also presented and discussed. For both array sizes we investigated the configuration when all obstacles are of uniform height and when the central obstacle is of double height. See Fig. 2 for schematics of the tested configurations and locations of the laser sheets for PIV measurements. The PIV technique measures velocity by correlating images of the particle-seeded flow. The neutrally buoyant Pliolite® particles (median diameter 50 μm) were illuminated in a plane using a laser sheet with a wavelength of 532 nm (with energy of 388 mJ/pulse) generated by a double-pulsed Nd:YAG laser (Big Sky Laser Technologies, Inc., model CFR400). The Q-switch was set to 120 μs corresponding to approximately medium laser power. The laser beam was expanded into a diverging light sheet using sheet-forming optics, which included the laser arm with three cylindrical lenses (each lens with 15 mm focal length) to achieve wide enough laser sheet to cover whole 3 × 3 array. A larger, 5 × 5 array had to be covered in parts. A LASERPULSE Synchronizer (TSI Inc., model 610034) was utilized to trigger the laser pulse and the camera with correct sequences and timing through a 2.66 GHz dual-processor workstation (Intel Xeon™). The laser sheet was synchronized with a high resolution (1600 × 1192 pixels) POWERVIEW 2M CCD camera (TSI Inc., model 630157) with a 50 mm f/1.8 Nikkor lens and an exposure time of 260 μs. The fields of view of the camera were 320 × 238 mm for the measurement in vertical plane, 380 × 283 mm for horizontal plane measurement of 3 × 3 arrays, and 190 × 142 mm for horizontal plane measurement of 5 × 5 arrays (5 × 5 arrays were covered part by part). Actual regions of interest in 3 × 3 arrays (Figs. 3–6), in which PIV was performed, were slightly smaller to avoid lens distorted edge image parts. The regions of interest for PIV processing of 5 × 5 arrays were only 60 × 60 mm (Figs. 7 and 8). Camera aperture was set to f/5.6. Time difference between the two images in a pair was optimized for the best PIV quality to Δt=1100 μs. A grid for the PIV processing was formed using the Nyquist Grid Engine over 32 by 32 pixels interrogation regions. Fast Fourier Transform correlation was used with the Gaussian Peak Engine. TSI Insight 3G software was used for the image conditioning and processing.

The uncertainty analysis was performed according to ITTC (2008) recommendations for PIV measurements. The uncertainty for velocity measurement results from the calibration (magnification) factor, α, image displacement ΔX, time interval Δt and lag of the tracer particle from the flow field, δu. Note that δu also accounts for measuring 3-D flow in 2-D plane. PIV velocity can be expressed as $u=\alpha\Delta X/\Delta t+\delta u$. From calibration images we determined α (units of α are mm pixel^{-1}, or short mm pxl^{-1}). Time interval Δt was optimized to 1.1 ms. Uncertainty in each of α, ΔX, Δt and δu results from several error sources (for details refer to ITTC, 2008). Sensitivity coefficients $(\partial u/\partial\Delta X, \partial u/\partial\Delta t, \partial u/\partial\alpha, \partial u/\partial\delta u)$ were calculated from measurements, taken from PIV software settings and our (TSI Inc.) PIV hardware specifications. Summarized results of uncertainty analysis for three camera views (vertical plane, horizontal 3 × 3 and horizontal 5 × 5) are given in Tables 1–3. Root-sum-square is employed for the accumulation of uncertainties. The combined uncertainty was estimated to be approximately 11%, 12% and 8% for vertical plane measurements, 3 × 3 horizontal measurements and 5 × 5 horizontal measurements, respectively.

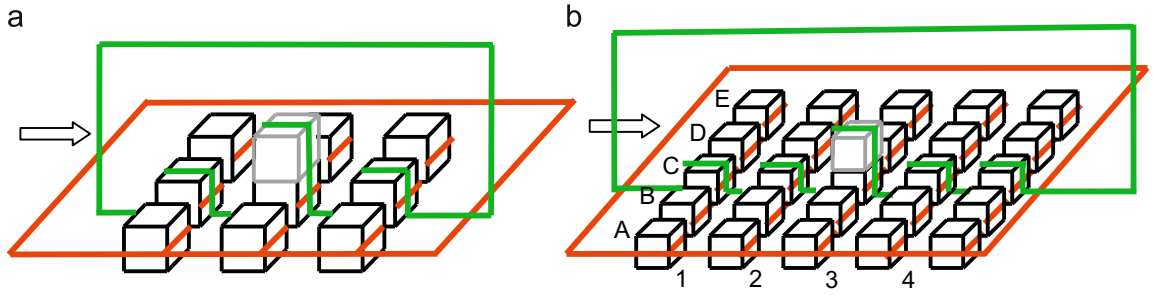

Fig. 2. Schematics of tested building array configurations: (a) 3×3 array of uniform height and with the tall central building (double height, shown in gray); (b) 5×5 array of uniform height and with the tall central building (double height, shown in gray). Green lines delineate vertical measurement plane and red lines delineate horizontal measurement plane. Arrows show the approaching flow direction. Capital letters A–E refer to array columns and numbers 1–4 refer to rows as used in Figs. 7 and 8. (For interpretation of the references to color in this figure legend, the reader is referred to the web version of this article.)

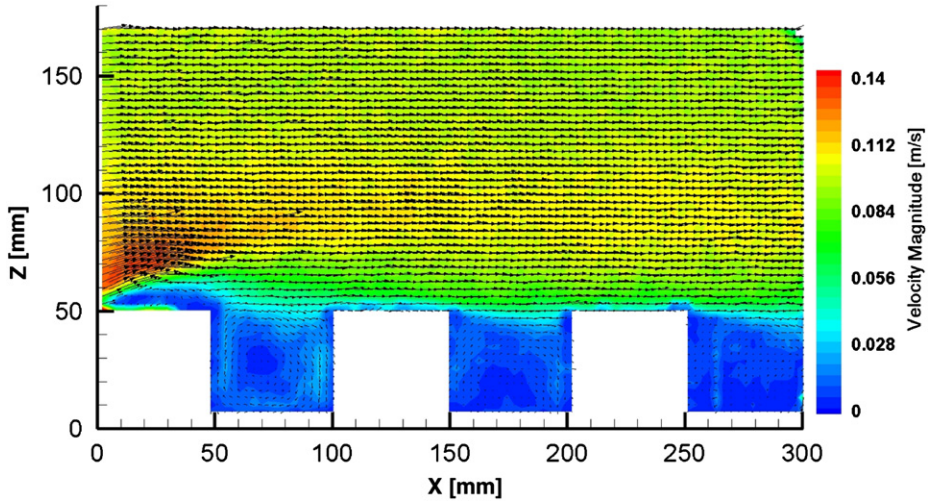

Fig. 3. Measured flow field in the vertical plane at the centerline of the uniform height array. Velocity magnitude color bar is given on the right.

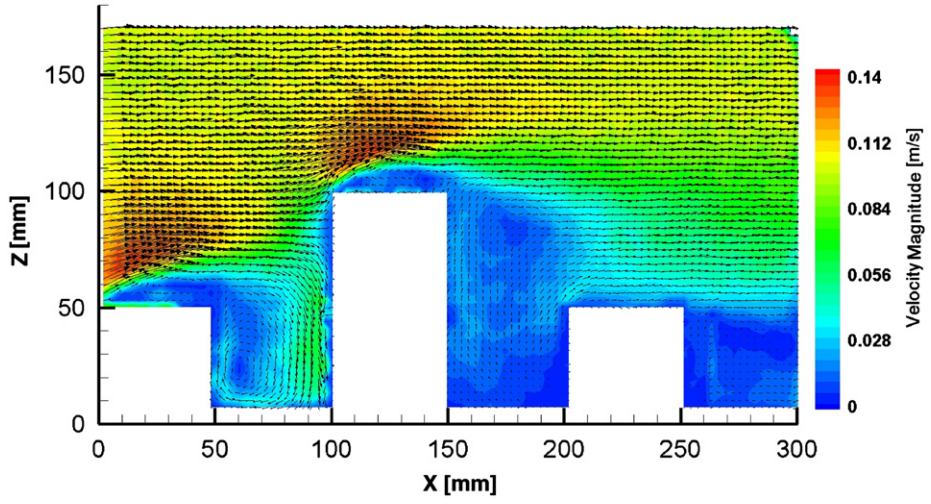

Fig. 4. Measured flow field in the vertical plane at the centerline of the array with tall central building. Note the strong downdraft caused by the tall building.

3.1. *Flow through a 3×3 array of cubes*

An array of 3×3 cubes was placed perpendicular to the flow in the channel test section. The cubes have H=5 cm long edges and the distance between cubes ("street width") was S=5 cm. The schematic of the experimental arrays and the measurement planes for vertical and horizontal flow fields is given in Fig. 2. The PIV measurements in the vertical plane confirmed well-known flow pattern. Flow field in the vertical plane through the array of uniform height, presented in Fig. 3, reveals expected acceleration regions at the leading edge of the first building and vortices behind each building row. For the case of tall central

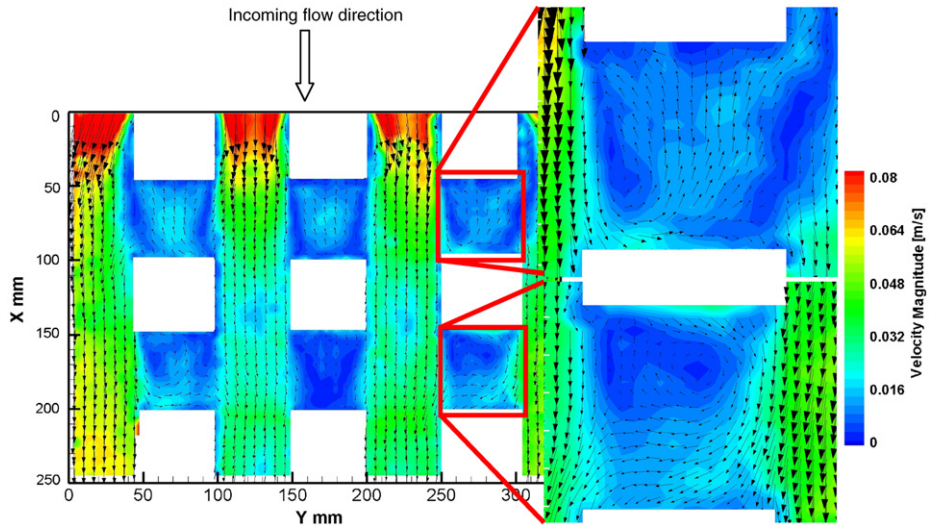

Fig. 5. Measured velocity field in the horizontal plane through a 3×3 building array of uniform height.

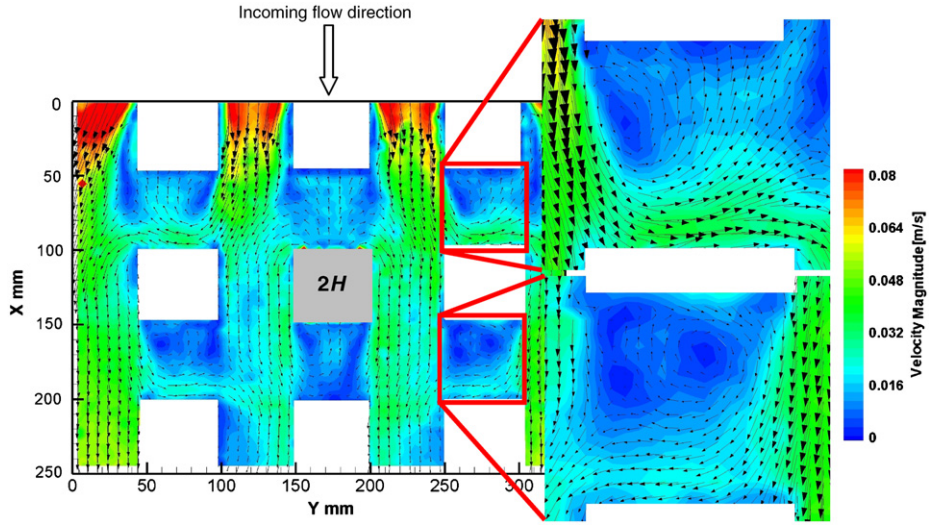

Fig. 6. Measured velocity field in the horizontal plane through a 3×3 building array with a central building of double height.

building (Fig. 4), in addition to the acceleration regions at the leading edges of the first building and the tall building, the blocking effect of the tall building is evident which results in intense downdraft and stronger vortex behind the first building.

A surprise came as we started to look at the detailed velocity field in the horizontal plane. The flow pattern through an array of regular obstacles is not something un-published. The typical published flow pattern would consist of the acceleration regions in the streets which are parallel to the incoming flow and the counter-rotating vortex pairs behind each building. However, that idealized picture does not match the actual flow through the three dimensional array. Here by "three dimensional" we refer to a finite array, not bounded with a wall on any side. The measured horizontal flow pattern is given in Fig. 5. As fluid enters the array it is partially deflected sideways after the first building row. It flows back into the array behind the second building row. This pattern, thereafter referred to as the "lateral channeling", was very surprising, and we suspected that there may be some problem in the experimental setup. The building alignment was checked and even the experiments with intentionally misaligned buildings in a way to oppose this pattern were performed. The influence of the channel walls was investigated and the buildings of half the original size (H=2.5 cm) were used to form the array. A range of Reynolds numbers was covered from Re=1000 to 7000. The pattern persisted and turned out to be insensitive to the building alignment imperfections and the incoming flow conditions (i.e. velocity profile and background turbulence).

The presented flow field in Fig. 5 is measured at $1/3H$ (1.6 cm) from the ground. The measurements were also performed at $1/2H$ and $2/3H$ from the ground level. The lateral channeling patterns, on both sides of the array, are symmetric along the array centerline and are independent of the measurement height. Since these measurements are close to the ground level (at $1/3H$), the back flow of the horizontal wake vortex can be seen in the lee of the central buildings.

The next step was to look at the influence of tall ($2H$) central building. Fig. 6 presents the flow pattern measured at the same location and under the same incoming flow conditions as the one given in Fig. 5 with the only difference being the tall central building. Note how the tall building causes more intense lateral outflow in the lee of the first row of buildings. This is a consequence of a strong downdraft caused by the blocking effect

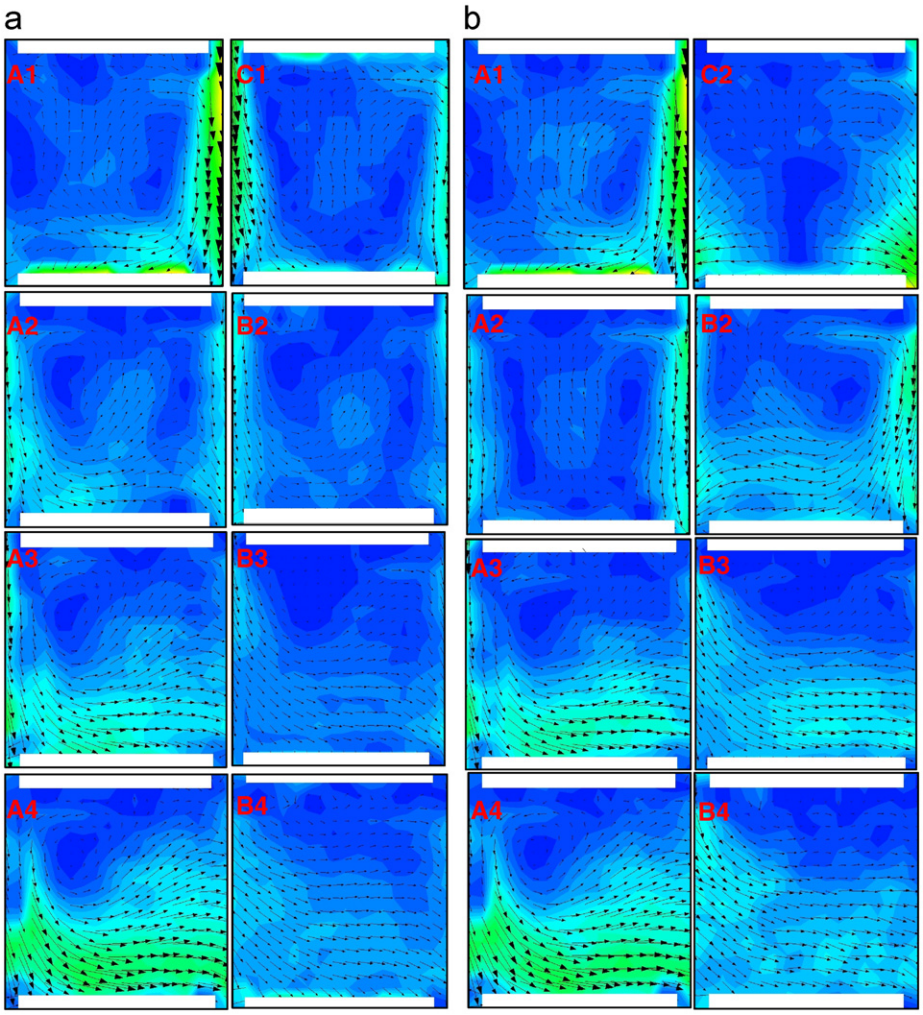

Fig. 7. (a) Measured horizontal velocity field within a uniform height 5×5 cubical array and (b) measured horizontal velocity field within a 5×5 cubical array with the central building of double height. Refer to Fig. 2 for location schematic. Velocity scale is given in Figs. 5 and 6.

of the tall building (see Fig. 4). The volumetric flow rate in the outflow region is three times larger than that in the outflow from the uniform height array.

3.2. *Flow through a 5×5 array of cubes*

We proceeded with the same measurements for a 5×5 array of cubes as presented by schematic in Fig. 2. The measured flow fields in representative regions of the uniform height array are given in Fig. 7a. Refer to schematic in Fig. 2b for location notation. Note again the lateral channeling from the array behind the first row of buildings (location A1). This is followed by the lateral channeling into the array in all following rows. In this case the introduction of a tall central building (Fig. 7b) could not significantly influence the lateral outflow channeling in the first row, which is one row upstream of it. However, as expected from our 3×3 array results, the lateral spreading of the downdraft near the ground caused by the tall building did block the lateral channeling into the array at the second row. Actually this lateral spreading of the tall building downdraft was strong enough to completely block the inflow in location A2 and fully reverse the flow direction from inflow to outflow in the columns next to the tall building (location B2). For clarity, we include plots of streamlines (Fig. 8) calculated directly from velocity vectors (Fig. 7).

4. Summary

A re-circulating water channel was utilized to create controlled flow field to model wind flows through simple mock urban environments. In this communication the flows through regular arrays of 3×3 and 5×5 cubical mock buildings are reported. A novel flow pattern within the array was observed in the horizontal plane. This flow pattern shows regions of lateral channeling in the form of the mean outflow from the array and the mean inflow into the array. For the case of the tall central building in 3×3 array this "sideway" flow is significantly enhanced, while the tall central building in 5×5 array causes the blockage, and reversal, of the inflow to the array.

The unavoidable question is why this flow pattern was not reported by the previous studies? Most of previous wind tunnel and water flume studies focused on quasi-2-D arrays, arrays that would cover the whole width of the test section allowing the channel walls to block any possible lateral flow channeling. The same distortion can be done by imposing the periodic boundary conditions (e.g. Coceal et al., 2006; Lien and Yee, 2004), which emulates the infinite array in lateral direction, for numerical simulations. Also, none of the previous researchers had the laboratory capabilities to perform such detailed and precise measurements of the flow between the obstacles. Even when the building array was not from side to side of the experimental facility, most measurements were point measurements using hot

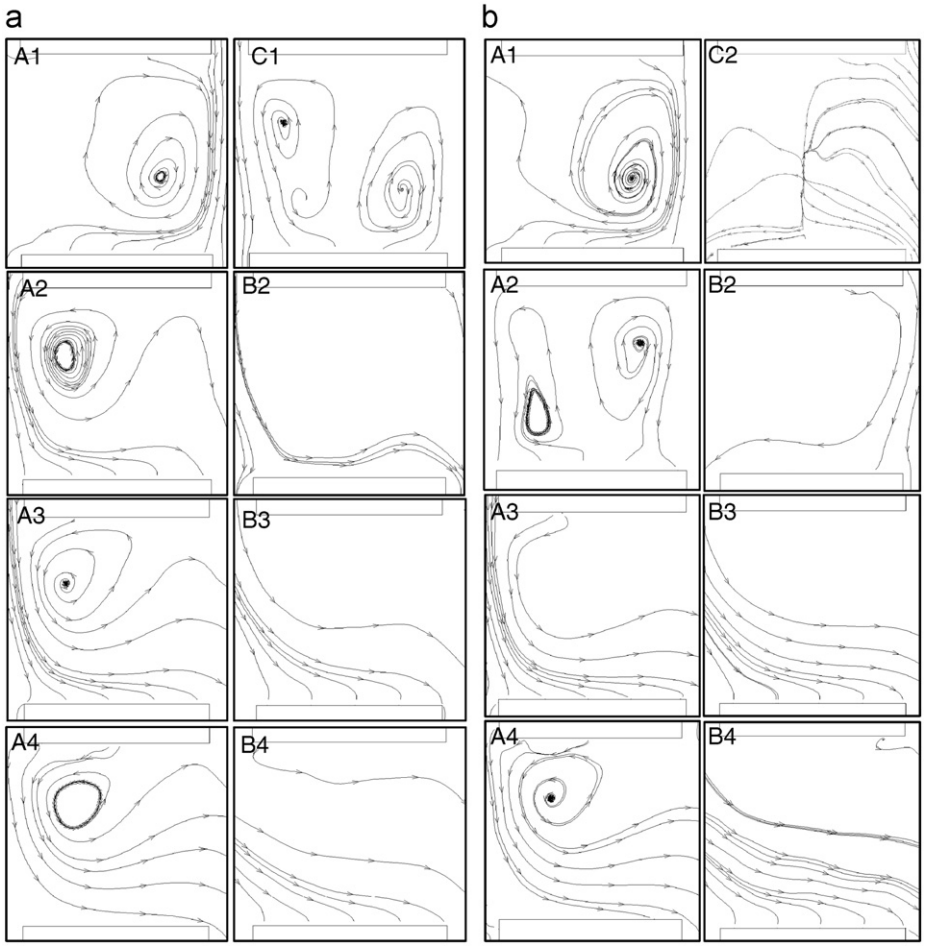

Fig. 8. (a) Streamlines calculated from velocity field in Fig. 7a for 5×5 array of uniform height and (b) streamlines calculated from velocity field in Fig. 7b for 5×5 array with a central building of double height. Refer to Fig. 2 for location schematic.

Table 1
Uncertainty for vertical plane measurements and free stream velocity of 8.2 cm/s.

Parameter	Uncertainty (u)	Sensitivity coefficient (c)	cu
α (mm pxl^{-1})	0.00114	41.0 (pxl s^{-1})	0.05 (mm s^{-1})
ΔX (pxl)	0.047	181.8 (mm pxl^{-1}s^{-1})	8.62 (mm s^{-1})
Δt (s)	5.39e−09	7.0 (m s^{-2})	0.00 (mm s^{-1})
δu (mm/s)	0.158	1.0	0.16 (mm s^{-1})
Combined uncertainty (root-sum-square)			8.63 (mm s^{-1})
Percentage uncertainty			10.52%

Table 2
Uncertainty for 3×3 array horizontal measurements and free stream velocity of 8.2 cm/s.

Parameter	Uncertainty (u)	Sensitivity coefficient (c)	cu
α (mm pxl^{-1})	0.00136	34.5 (pxl s^{-1})	0.05 (mm s^{-1})
ΔX (pxl)	0.045	215.9 (mm pxl^{-1}s^{-1})	9.82 (mm s^{-1})
Δt (s)	5.39e−09	7.0 (m s^{-2})	0.00 (mm s^{-1})
δu (mm/s)	0.189	1.0	0.19 (mm s^{-1})
Combined uncertainty (root-sum-square)			9.82 (mm s^{-1})
Percentage uncertainty			11.98%

wires, pressure transducers, Pitot tubes or line measurements using the scanning laser Doppler velocimetry (LDV), and none was able to "see-through" the obstacles/buildings.

Table 3
Uncertainty for 5×5 array horizontal measurements and free stream velocity of 8.2 cm/s.

Parameter	Uncertainty (u)	Sensitivity coefficient (c)	cu
α (mm pxl^{-1})	0.00068	69.1 (pxl s^{-1})	0.05 (mm s^{-1})
ΔX (pxl)	0.058	108.0 (mm pxl^{-1}s^{-1})	6.29 (mm s^{-1})
Δt (s)	5.39e−09	7.0 (m s^{-2})	0.00 (mm s^{-1})
δu (mm/s)	0.093	1.0	0.09 (mm s^{-1})
Combined uncertainty (root-sum-square)			6.29 (mm s^{-1})
Percentage uncertainty			7.68%

This study shows that approximating even very simple 3-D flow configurations with a quasi-3-D (e.g. periodic boundaries in numerical simulations, or wall bounded arrays in experiments) can lead to deceptive results. Flow displacement, acceleration and separation occur not only above the array but also on the array sides, which become impossible for the sidewall bounded arrays. For the neutral atmosphere there is no reason to give preference neither to the array side acceleration nor above the array acceleration. For the stable case the vertical rising would be blocked giving even more weight to the flow acceleration around the array rather than above it.

Purely physical explanation of the lateral channeling can be given in the following way.

Outflow behind the first row of buildings: One can imagine a second row of obstacles replaced with a single array-wide block.

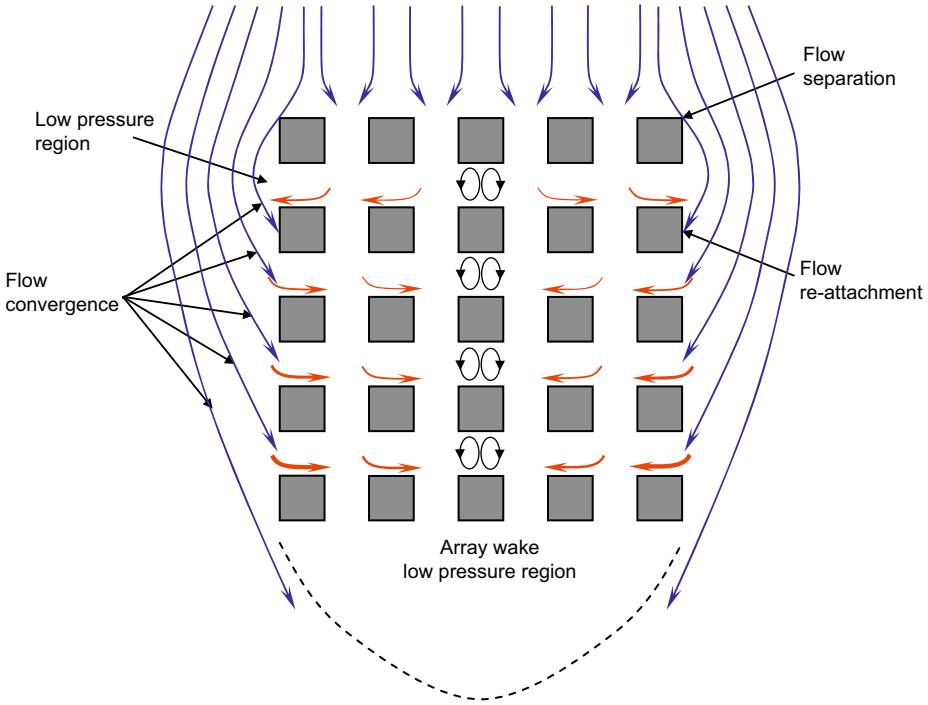

Fig. 9. Schematic of streamlines (blue) of the flow around a 5×5 cubical array. Red arrows represent the lateral channeling inside the array. Thickness of red lines corresponds to the relative flow intensity. Wake behind obstacles in the middle column consists of two counter rotating vortices. Case of uniform obstacle height is presented. For the case of tall central building flow behind the second row will change (refer to Fig. 7b, locations A2 and B2). (For interpretation of the references to color in this figure legend, the reader is referred to the web version of this article.)

Obviously, the flow in this case would diverge around the block. Now, let us imagine a block with small gaps. If the gaps in the block are not big enough, in addition to the small amount of flow through the gaps, we will still have the flow divergence in front of the block. Following this logic one can see the second row of buildings as a big block with big gaps that still gives fairly strong longitudinal flow resistance to promote the lateral channeling: outflow in the first street. Further, as flow approaches the array, separation occurs at the leading edge of side buildings in the first row and reattachments occurs further downstream (see measurements in Fig. 5). This flow separation exposes the first lateral street to low pressure regions on both array sides, which enhances the outflow (see schematic on Fig. 9).

Inflow in the remaining part of the array: Streamlines that are deflected by the array, in front of it, are converging back towards the array center forming inflows to the array (Fig. 9). In addition, low pressure in the wake region draws the fluid through the array. This wake low pressure leads to formation of the strongest lateral inflow in front of the last row of buildings. As rows are further from the wake region inflow is less intense due to decreased pressure gradient.

In summary, combination of streamline convergence towards the array, pressure field caused by flow separation at the leading edge and in the array wake together with the increased flow resistance through the array, leads to the lateral channeling (Fig. 9). Presence of a tall central building will cause downdraft whose divergence at the ground level can completely overcome inflow to the array before the central row.

With this physical explanation in mind, the current results allow us to speculate that the mean lateral flows into and out of the array will be prominent for arrays of regular and equidistant obstacles with length (dimension parallel to the wind direction) comparable or larger than the array width (dimension perpendicular to the wind direction, i.e. lateral). Future work has to include the investigation of lateral channeling sensitivity to the array length/width parameter and *S*/*H* ratio. At this moment we can speculate that the lateral outflow in the first street is proportional to the array length/width ratio due to the increased flow resistance through the array for longer arrays. This should be valid for the skimming regime and it is probably not valid for the isolated and wake interference regimes. Due to the cost of laboratory experiments we plan to investigate this systematically using a computational fluid dynamics (CFD) model. It should be noted that the CFD model was already deployed to the same building configuration as the laboratory experiments. Assuming neutral atmosphere, logarithmic velocity profile with a roughness length of $z_0 = 0.05$ m is used as the incoming wind. Reference velocity was $U = 5\,\mathrm{m\,s^{-1}}$ at the 10 m height. Cubical building height was also $H = 10$ m for all simulations. Zero shear condition is used at the domain boundaries. In this way, the model was run at very high $Re \sim 3 \times 10^6$ eliminating any possibility that the observed pattern is some laboratory, low *Re* artifact. The model reproduced the measured flow patterns. Detailed comparisons of CFD and laboratory results will be presented separately.

As mentioned in the introduction, compared to plumes in the open terrain, the plumes in the arrays are wider (Macdonald et al., 2000a, b; Macdonald, 2000), making initial spread very abruptly as entering the array. A question remains: Can this flow pattern, specifically the lateral outflow in the lee of the first building row, explain the sudden plume spread as it enters the array of obstacles? This is highly likely the case, but it is too early for such conclusion. Dispersion experiments using simultaneous PIV and the Planar Laser Induced Fluorescence (PLIF) measurements are needed to investigate the actual plume spread through these arrays.

Acknowledgments

This work was supported by the Los Alamos National Laboratory, Contract number 38510-001-06. The authors are very grateful to Dr. Michael Brown for invaluable discussions and comments and to two anonymous reviewers for invaluable comments. J.-J. Baik was supported by the Korea Meteorological Administration Research and Development Program under Grant CATER 2006-2202.

References

Adrian, R.J., 1988. Review of particle image velocimetry research. In: The Symposium on Optical Methods in Flow and Particle Diagnostics, Sixth International Congress on Applications of Lasers and Electro-Optics, San Diego, CA, Opt. Lasers Eng., vol. 9, pp. 317–319.

Adrian, R.J., 1991. Particle-imaging techniques for experimental fluid-mechanics. Ann. Rev. Fluid Mech. 23, 261–304.

Adrian, R.J., 1997. Dynamic ranges of velocity and spatial resolution of particle image velocimetry. Meas. Sci. Technol. 8 (12), 1393–1398.

Allwine, K.J., Shinn, J.H., Streit, G., Clawson, K., Brown, M., 2002. Overview of URBAN 2000. Bull. Am. Meteorol. Soc. 83 (4), 521–536.

Allwine, K.J., Clawson, K.J., Leach, M., Burrows, D., Wayson, R., Flaherty, J., Allwine, E., 2004. Urban dispersion processes investigated during the Joint Urban 2003 study in Oklahoma City. In: Proceedings of the Fifth AMS Symposium on the Urban Environment, Vancouver, B.C.

Allwine, K.J., Flaherty, J.E., 2006. Urban dispersion program MSG05 field study: summary of tracer and meteorological measurements. Pacific National Laboratory Report, PNNL-15969, 27p.

Aly, K.M., Esmail, E., 1993. Refractive index of salt water: effect of temperature. Opt. Mater. 2, 195–199.

Baik, J.-J., Park, R.S., Chun, H.Y., Kim, J.J., 2000. A laboratory model of urban street-canyon flows. J. Appl. Meteorol. 39, 1592–1600.

Biltoft, C., 2001. Customer report for mock urban setting test. Report No. WDTC-FR-01-121, US Army Dugway Proving Ground.

Brown, M., Lawson, R., DeCroix, D., Lee, R., 2001. Comparison of centerline velocity measurements obtained around 2D and 3D building arrays in a wind tunnel. In: Proceedings of the Environmental Hydraulics, Tempe, AZ.

Cheng, H., Castro, I.P., 2002a. Near-wall flow development after a step change in surface roughness. Boundary-Layer Meteorol. 105, 411–432.

Cheng, H., Castro, I.P., 2002b. Near-wall flow over urban-like roughness. Boundary-Layer Meteorol. 104, 229–259.

Coceal, O., Thomas, T.G., Castro, I.P., Belcher, S.E., 2006. Mean flow and turbulence statistics over groups of urban-like cubical obstacles. Boundary-Layer Meteorol. 121, 491–519.

Dabberdt, W., Hoydysh, W., 1991. Street canyon dispersion: sensitivity to block shape and entrainment. Atmos. Environ. 25A, 1143–1153.

Eliasson, I., Offerle, B., Grimmond, C.S.B., Lindqvist, S., 2006. Wind fields and turbulence statistics in an urban street canyon. Atmos. Environ. 40, 1–16.

Fernando, H.J.S., Lee, S.-M., Anderson, J., Princevac, M., Pardyjak, E., Grossman-Clarke, S., 2001. Urban fluid mechanics: air circulation and contaminant dispersion in cities. Environ. Fluid Mech. 1, 107–164.

Finnigan, J.J., Belcher, S.E., 2004. Flow over a hill covered with a plant canopy. Q. J. R. Meteorol. Soc. 130 (596), 1–29 Part A.

Gavze, E., Fattal, E., Pistinner, S., 2002. Turbulence properties of the street-roof scale within the urban roughness sub-layer. In: Proceedings of the Fourth AMS Symposium on the Urban Environment, Norfolk, VA.

Hosker, R.P., 1980. The effects of buildings on local dispersion, Atmospheric turbulence and diffusion laboratory, National Oceanic and Atmospheric Administration, Oak Ridge, TN 37830.

Hoydysh, W., Dabberdt, W., 1988. Kinematics and dispersion characteristics of flows in asymmetric street canyons. Atmos. Environ. 22, 2677–2689.

International Towing Tank Conference (ITTC), 2008. Uncertainty analysis: particle image velocimetry, 7.5-01-03-03, 12pp, September 2008.

Kastner-Klein, P., Plate, E., Fedorovich, E., 1997. Gaseous pollutant dispersion around urban-canopy elements: wind-tunnel case studies. Int. J. Environ. Pollut. 8, 727–737.

Kastner-Klein, P., Plate, E., 1999. Wind-tunnel study of concentration fields in street canyons. Atmos. Environ. 33 (24–25), 3973–3979.

Kastner-Klein, P., Fedorovich, E., Rotach, M., 2001. A wind tunnel study of organized and turbulent air motions in urban street canyons. J. Wind Eng. Ind. Aerodyn. 89, 849–861.

Kastner-Klein, P., Rotach, M.W., 2004. Mean flow and turbulence characteristics in an urban roughness sublayer. Boundary-Layer Meteorol. 111 (1), 55–84.

Kastner-Klein, P., Berkowicz, R., Britter, R., 2004. The influence of street architecture on flow and dispersion in street canyons. Meteorol. Atmos. Phys. 87 (1–3), 121–131.

Lien, F.S., Yee, E., 2004. Numerical modelling of the turbulent flow developing within and over a 3-D building array, part I: a high-resolution Reynolds-averaged Navier–Stokes approach. Boundary-Layer Meteorol. 112 (3), 427–466.

Lien, F.S., Yee, E., Wilson, J.D., 2005. Numerical modelling of the turbulent flow developing within and over a 3-D building array, part II: A mathematical foundation for a distributed drag force approach. Boundary-Layer Meteorol. 114 (2), 245–285.

Macdonald, R.W., Hall, D., Walker, S., Spanton, A., 1998. Wind tunnel measurements of wind speed in simulated urban arrays. BRE Report CR-243/98, 50pp.

Macdonald, R.W., 2000. Modelling the mean velocity profile in the urban canopy layer. Boundary-Layer Meteorol. 97, 25–45.

Macdonald, R.W., Carter, S., Slawson, P.R., 2000a. Measurements of mean velocity and turbulence statistics in simple obstacle arrays at 1:200 scale. Thermal Fluids Report.

Macdonald, R.W., Coulson, B.J., Slawson, P.R., 2000b. Near field dispersion in the urban environment—a hydraulic flume study. Environ. Monit. Assessment 65 (1–2), 231–238.

Macdonald, R.W., Carter, S., Slawson, P., 2002. Physical modeling of urban roughness using arrays of regular roughness elements. Water Air Soil Pollut. 2, 541–554.

Oke, T.R., 1987. Boundary Layer Climates, second ed. Routledge, London.

Pavageau, M., Schatzmann, M., 1999. Wind tunnel measurements of concentration fluctuations in an urban street canyon. Atmos. Environ. 33 (24–25), 3961–3971.

Prasad, A.K., Adrian, R.J., Landreth, C.C., Offutt, P.W., 1992. Effect of resolution on the speed and accuracy of particle image velocimetry interrogation. Exp. Fluids 13 (2–3), 105–116.

Rafailidis, S., Schatzmann, M., 1995. Concentration measurements with different roof patterns in street canyons with aspect ratios $B/H=1/2$ and $B/H=1$. Report, Universitat Hamburg, Meteorologisches Institut.

Rotach, M.W.L., Vogt, R., Bernhofer, C., Batchvarova, E., Christen, A., Clappier, A., Feddersen, B., Gryning, S.E., Martucci, G., Mayer, H., Mitev, V., Oke, T.R., Parlow, E., Richner, H., Roth, M., Roulet, Y.A., Ruffieux, D., Salmond, J.A., Schatzmann, M., Voogt, J.A., 2005. BUBBLE—an urban boundary layer meteorology project. Theor. Appl. Climatol. 81 (3–4), 231–261.

Schatzmann, M., Leitl, B., Liedtke, J., 2000. Dispersion in urban environments—comparison of field measurements with wind tunnel results. Environmental Monitoring and Assessment 65 (1–2), 249–257.

Shavit, U., Brandon, T., 2001. Dispersion within emergent vegetation using PIV and concentration measurements. In: Proceedings of the Fourth International Symposium on Particle Image Velocimetry Gottingen, Germany, pp. 17–19.

Takahashi, A., Hiyama, T., 2004. A momentum exchange model for the surface layer over bare-soil and canopy-covered surfaces. J. Appl. Meteor. 43 (10), 1460–1476.

Theurer, W., Plate, E.J., Höschele, K., 1996. Semi-empirical models as a combination of wind tunnel and numerical dispersion modelling. Atmos. Environ. 30, 3583–3597.

Theurer, W., 1999. Typical building arrangements for urban air pollution modelling. Atmos. Environ. 33, 4057–4066.

Venkatram, A., Isakov, V., Pankratz, D., Heumann, J., Yuan, J., 2005. Relating plume spread to meteorology in urban areas. Atmos. Environ. 39 (2), 371–380.

Wedding, J., Lombardi, D., Cermak, J., 1977. A wind-tunnel study of gaseous pollutants in city street canyons. J. Air Pollut. Control Assoc. 27, 557–566.

Yamartino, R.J., Wiegand, G., 1986. Development and evaluation of simple models for the flow, turbulence, and pollutant concentration fields within an urban street canyon. Atmos. Environ. 20, 2137–2156.

Yee, E., Gailis, R.M., Hill, A., Hilderman, T., Kiel, D., 2006. Comparison of wind-tunnel and water-channel simulations of plume dispersion through a large array of obstacles with a scaled field experiment. Boundary-Layer Meteorol. 121, 389–432.

Yuan, J., Venkatram, A., 2005. Dispersion within a model urban area. Atmos. Environ. 39 (26), 4729–4743.